ACSNANO

www.acsnano.org

ARTICLE

A Breathable, Reusable, and Zero-Power Smart Face Mask for Wireless Cough and Mask-Wearing Monitoring

Zhilu Ye,[‖] Yun Ling,[‖] Minye Yang, Yadong Xu, Liang Zhu, Zheng Yan,* and Pai-Yen Chen*

Cite This: *ACS Nano* 2022, 16, 5874−5884

Read Online

ACCESS | Metrics & More | Article Recommendations | Supporting Information

ABSTRACT: We herein introduce a lightweight and zero-power smart face mask, capable of wirelessly monitoring coughs in real time and identifying proper mask wearing in public places during a pandemic. The smart face mask relies on the compact, battery-free radio frequency (RF) harmonic transponder, which is attached to the inner layer of the mask for detecting its separation from the face. Specifically, the RF transponder composed of miniature antennas and passive frequency multiplier is made of spray-printed silver nanowires (AgNWs) coated with a poly(3,4-ethylenedioxythiophene):poly(styrenesulfonate) (PEDOT:PSS) passivation layer and the recently discovered multiscale porous polystyrene-*block*-poly(ethylene-*ran*-butylene)-*block*-polystyrene (SEBS) substrate. Unlike conventional on-chip or on-board wireless sensors, the SEBS-AgNWs/PEDOT:PSS-based RF transponder is lightweight, stretchable, breathable, and comfortable. In addition, this wireless device has excellent resilience and robustness in long-term and repeated usages (i.e., repeated placement and removal of the soft transponder on the mask). We foresee that this wireless smart face mask, providing simultaneous cough and mask-wearing monitoring, may mitigate virus-transmissive events by tracking the potential contagious person and identifying mask-wearing conditions. Moreover, the ability to wirelessly assess cough frequencies may improve diagnosis accuracy for dealing with several diseases, such as chronic obstructive pulmonary disease.

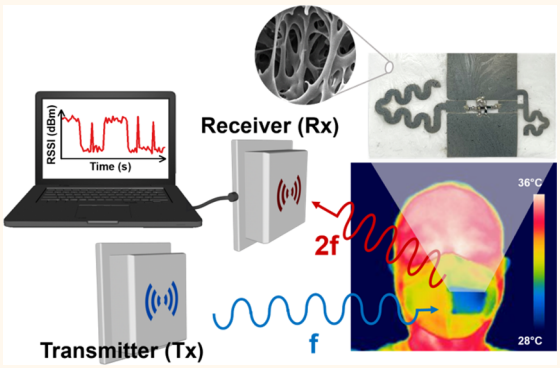

KEYWORDS: *flexible electronics, wearable electronics, nanowires, porous composite, smart face mask*

The coronavirus disease 2019 (COVID-19), a respiratory epidemic that caused significant morbidity and even mortality, has widely spread worldwide since the detection of the first case in 2019. So far, this global pandemic has given rise to more than 400 million confirmed cases and 6 million deaths around the world,[1] concurrent with psychological, social, and economic complications. To mitigate the devastating impact of COVID-19, a number of measures were suggested, such as hand hygiene, social distancing, quarantine, and vaccination.[2] Perhaps, face mask wearing enforcement in densely populated places is one of the most effective means to stop the spread of virus, as respiratory face masks are highly effective in blocking most respiratory droplets and aerosols.[3,4] Despite these efforts, the increase in reported cases of COVID-19 continues, which has led to an urgent need for more effective ways to combat the coronavirus and restore society to a certain semblance of normalcy. To address this, smart face masks made by equipping respiratory face masks with electronic sensors and modules have been recently proposed.[5−9] To date, smart masks are mainly used for two purposes: (1) to monitor respiratory symptoms, such as cough,[5−7,10] and (2) to enhance the filtration of airborne pathogens including coronaviruses;[8,9,11] both contribute to prevention and control of respiratory diseases. In addition to the significance in diminishing the pandemic, there has been a witnessed trend of smart masks and wearables for their potential in health monitoring and preventive care,[12−16] personalized behavior modeling,[17−20] and healthcare internet-of-things (IoTs).[21−26] Nevertheless, existing research largely ignores wearing comfort and breathability, which are crucial for user experience and compliance of wearing face masks. The state-of-the-art smart face masks usually employ rigid materials

Received: December 12, 2021
Accepted: March 15, 2022
Published: March 17, 2022

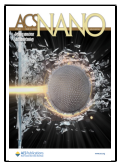

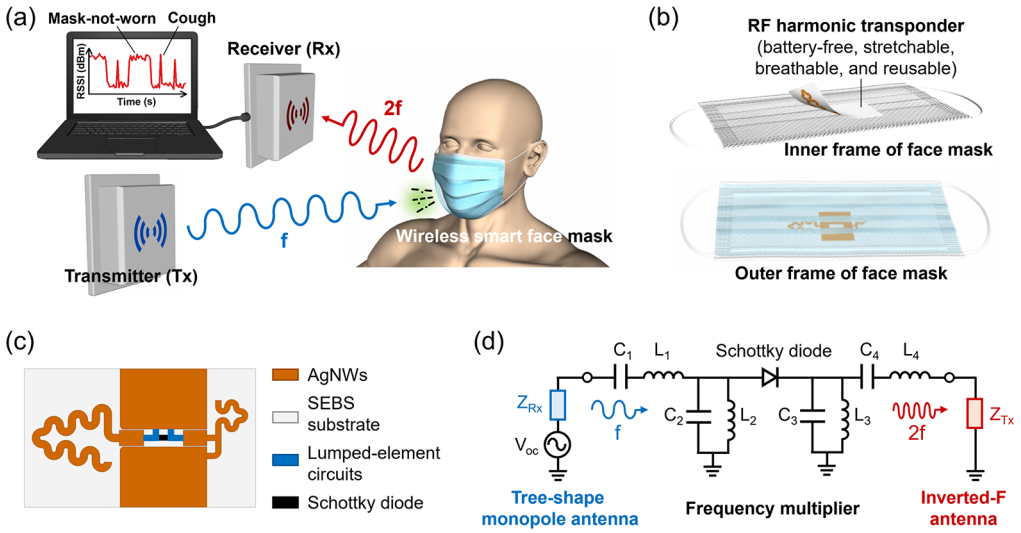

Figure 1. (a) Schematic of the smart face mask equipped with a harmonic transponder. When cough occurs and/or face mask is not worn properly, the smart mask is capable of receiving the interrogation signal (*f*) from the transmitting antenna (Tx) and retransmitting the modulated harmonic signal (2*f*) to the receiving antenna (Rx). (b) Diagram of the smart face mask formed by an ordinary face mask and a soft harmonic transponder attached to its inner layer. (c) Geometry and (d) circuit diagram of the harmonic transponder, which consists of a tree-shaped monopole antenna, a frequency multiplier, and a curved inverted-F antenna. See Supporting Information for detailed design parameters.

or printed circuit boards (PCBs) attached to the nonporous polydimethylsiloxane (PDMS),[5,7−9,21,27] which are generally bulky, cumbersome, and, most importantly, nonbreathable. The lack of breathability markedly impedes the practice of smart face masks due to swelter and discomfort. In addition, the devices attached to the smart face mask may scratch the face in some scenarios. As a result, to develop a fully stretchable, breathable, and biocompatible smart mask sensor with thermal management ability (e.g., passive cooling) has both clinical and practical significance.

In this work, we present a multifunctional wireless smart mask, capable of identifying mask-wearing conditions and monitoring the frequency and pattern of coughing (i.e., a common symptom of many respiratory diseases)[28,29] (Figure 1a). The proposed smart face mask consists of a zero-power radio frequency (RF) harmonic transponder, which is attached to the inner side of an ordinary face mask and can be torn off and reattached for repeated usage (Figure 1b). To achieve better wearing comfort than current smart masks,[5−11,21,27] the RF harmonic transponder is printed using spray-printed silver nanowires (AgNWs) on the multiscale porous polystyrene-*block*-poly(ethylene-*ran*-butylene)-*block*-polystyrene (SEBS) substrate (Figure 1c); both nanomaterials are lightweight, flexible, stretchable, and, most importantly, breathable. Moreover, the 0.2−7 μm pores of the SEBS substrate can efficiently block the sunlight, while allowing transmission of the human-body infrared (IR) radiation (which is in some sense similar to a spectral filter), thereby enabling passive heat dissipation and/or passive cooling.[30] Along with its water-resistant ability,[30] the porous SEBS substrate has broadened the application of the proposed smart masks in scorching weather or moderate-intensity rain. We also sprayed a layer of poly(3,4-ethylenedioxythiophene):poly(styrenesulfonate) (PEDOT:PSS) as a passivation layer to improve the stability and durability of the AgNWs in air and humid conditions. It is noted that both the SEBS substrate and the conductive materials (AgNWs and PEDOT:PSS) are biocompatible and environmentally friendly, thereby being particularly suitable for wearable electronic applications.[16,20,31,32] To get rid of unwanted electromagnetic interferences, such as clutters, crosstalks, and self-jamming, the soft RF transponder, upon receiving an RF signal, retransmits its second harmonic, such that the frequency orthogonality can effectively eliminate the above interferences (Figure 1a,d).[14,15,33−43] In this vein, real-time monitoring of coughing and appropriate use of face masks can be achieved even in noisy indoor and rich-scattering environments. In addition, the soft harmonic transponder can be continuously used for at least 8 h and can be repeatedly used for at least 10 times, providing a cost-saving and ecofriendly solution. This zero-power, lightweight, and comfortable smart face mask with the wireless sensing function can not only alert when the face mask is incorrectly worn in public places but also monitors the cough frequency and patterns of the user to analyze respiratory symptoms (which can be mapped to the risk level of specific diseases via intelligent algorithms),[44−46] thereby mitigating the transmission of infectious respiratory diseases.

RESULTS AND DISCUSSION

Material Characteristics and Properties. The soft harmonic transponder embedded in the face mask takes advantage of the ultrasoft, flexible, stretchable, and breathable SEBS substrate with multiscale porous structures, which has been recently reported in our parallel work.[30] Figure 2a shows the fabrication process of the harmonic transponder, where the AgNWs and PEDOT:PSS were sequentially sprayed on a prestretched SEBS by an airbrush with shadow mask assist. After the conductive materials dried, the wireless transponder was released from the stretcher to form a crumpled conductive surface structure (Figure 2b). AgNWs have excellent performances in conductivity and biocompatibility, supporting the possibility of smart wearable electronics; however, one shortcoming that remains is the conductive instability in air due to oxidation and sulfidation of AgNWs.[47] On the other hand, the potential inhaled risk of AgNWs has been reported,

https://doi.org/10.1021/acsnano.1c11041
ACS Nano 2022, 16, 5874−5884

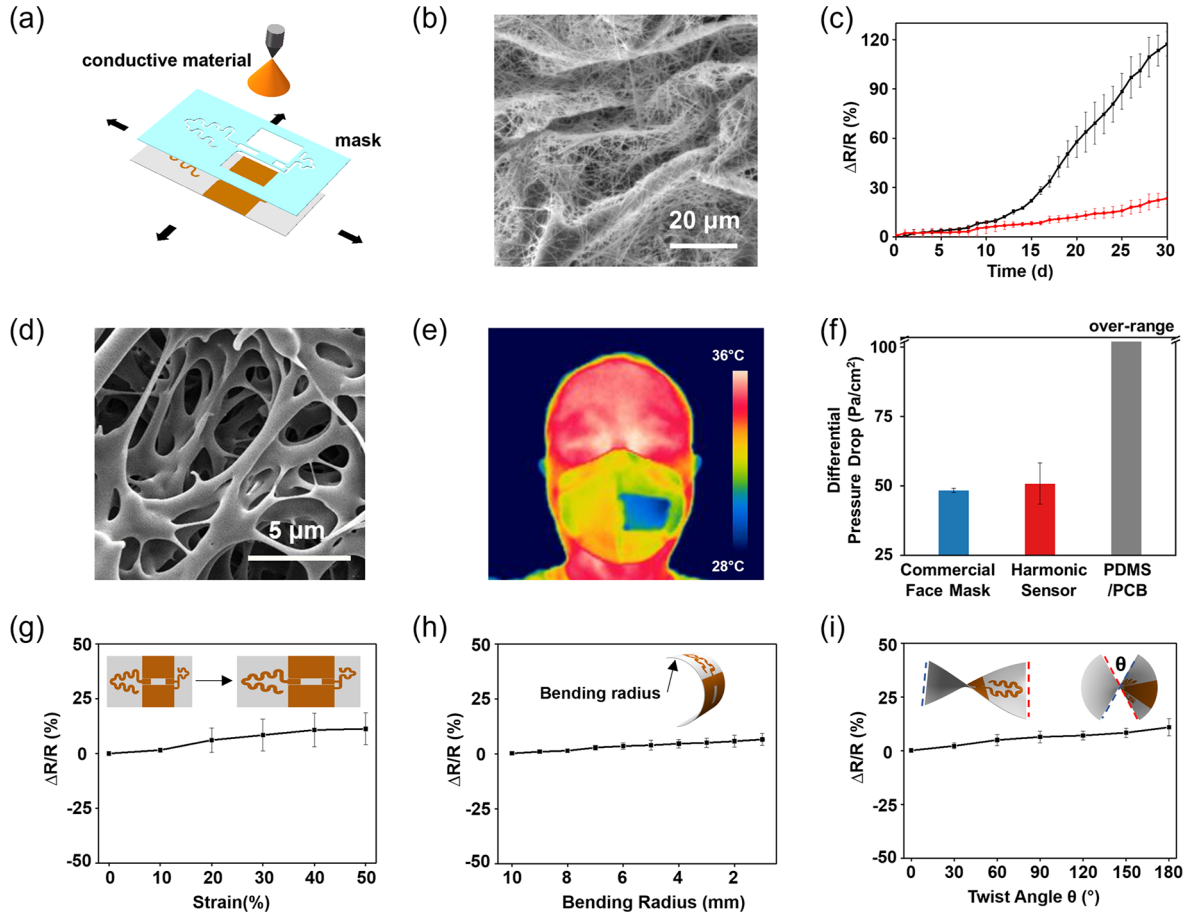

Figure 2. Characterization of a harmonic transponder made of PEDOT:PSS-coated AgNWs and multiscale porous SEBS substrate. (a) Scheme of the fabrication process. The SEBS substrate is prestretched and patterned conductive materials with shadow mask assist. (b) Crumpled structure of PEDOT:PSS-coated AgNWs on the surface of porous SEBS substrate (under 100% biaxial prestrain). (c) Electrical stability of AgNWs with (red) and without (black) PEDOT:PSS coating under 90% RH for 30 days. (d) SEM image of SEBS's intrinsic micron-scale porous structures. (e) IR image of people wearing the smart mask with the harmonic sensor attached; the temperature difference is about 3 °C. (f) Comparison of differential pressure drops of the commercial face mask, porous SEBS substrate of our designed harmonic sensor, and PDMS and/or PCB commonly used in current smart face masks.[5,7−9,21,27] Resistance changes under (g) stretching, (h) bending, and (i) torsion. The error bars are generated from 3 different samples in each group.

indicating that inhaled AgNWs may cause lung inflammation.[48] For those reasons, we choose a highly biocompatible conductive material PEDOT:PSS as the passivation layer to isolate the AgNWs and prevent leakage. PEDOT:PSS-coated AgNWs have strong bonding to the SEBS substrate, so that it would be hardly possible for the nanomaterials to fall off from the substrate surface. We use airflow with a speed of ∼3.0 m/s (which is much higher than the speed of human respiratory airflow) to blow the sensor surface to scotch tape overnight. The surface of the scotch tape is then observed by scanning electron microscope (SEM) with the result shown in Supporting Information (Figure S1). We find no AgNWs or conductive composite flakes blown onto the scotch tape. The experiment demonstrates the strong interface between the conductive materials and the SEBS substrate as well as the negligible risk of breathing in the nanomaterials. Based on the SEM cross-sectional image (see Figure S2), the thickness of the conductive material is estimated to be about 0.3 μm. The sheet resistance of the conductive material (determined by Ossila sheet resistance test platform) is 1 Ω/□ with a 13.2% standard deviation calculated from a group of 10 different samples. For the same sample, the resistance shows a 1.2% standard deviation when consecutively measured from 5 different positions, primarily due to the inconsistency of airbrush spray. This slight deviation does not affect the performance of the transponder sensor, as verified by our following experiments. In practical use, the relative humidity (RH) enclosed by the face mask could reach saturation (≥100%),[49] which also challenges the AgNWs' stability and the transponder's water-resistant ability. To address this concern, measurements of AgNWs' electrical stability ($\Delta R/R$) are performed, with results shown in Figure 2c. The harmonic transponder was stored at 90% RH (by saturated KNO_3 solution) and 32 °C for 30 days, to mimic the high humidity and warm environment. The sheet resistance of the conductive material (which is originally around 1 Ω/□) increases gradually due to the effect of high humidity and temperature. It is evidently seen from Figure 2c that the naked AgNWs (black line) show a ∼120% resistance increase, while the resistance of the PEDOT:PSS-coated group (red line) increases only ∼23%. This indicates that the passivation layer greatly improves the electrical stability of AgNWs and avoids potential inhalation risk, which makes the wireless harmonic transponder more durable and safe for use in smart face masks.

Wearing a face mask in hot weather is very likely to cause heat stress (e.g., heat stroke, heat exhaustion, etc.), which poses

https://doi.org/10.1021/acsnano.1c11041
ACS Nano 2022, 16, 5874−5884

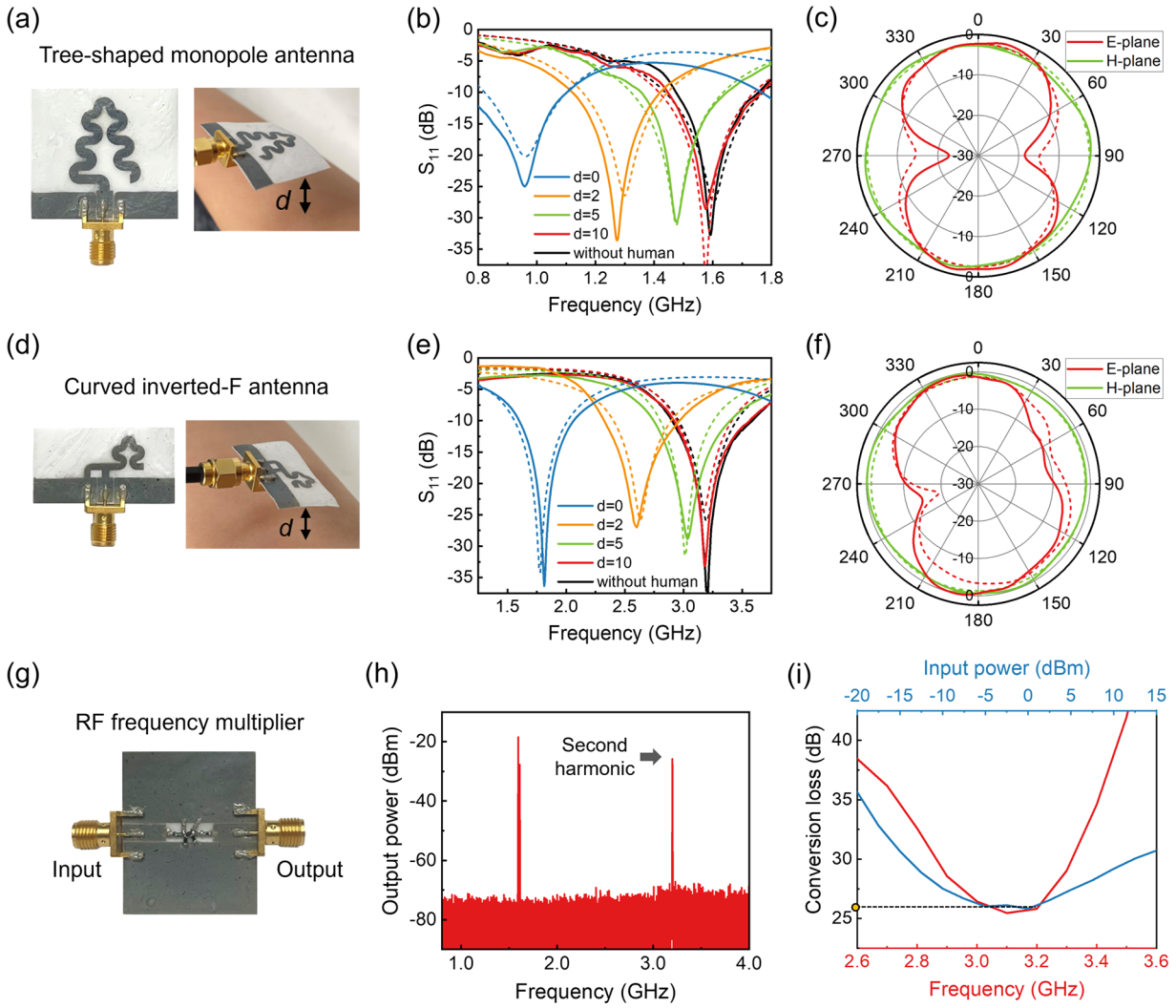

Figure 3. (a) Photographs of the fabricated tree-shaped monopole antenna (left) made of PEDOT:PSS-coated AgNWs and SEBS substrate and the measurement of reflection coefficients (right). (b) Measured (solid lines) and simulated (dashed lines) reflection coefficients S_{11} of the tree-shaped monopole antenna with different distances d between antenna and human body. (c) Radiation pattern of the tree-shaped monopole antenna at 1.6 GHz, where the experiment and simulation results are presented by solid and dashed lines, respectively. (d–f) Similar to (a–c) but for the curved inverted-F antenna (3.2 GHz). (g) Photograph of the fabricated RF frequency multiplier and (h) its output spectrum with input power of 0 dBm at 1.6 GHz. A second-harmonic signal can be clearly observed at 3.2 GHz. (i) Measured conversion loss of the frequency multiplier at different input frequencies (red line) and different input lower levels (blue line).

a severe threat to people under high-temperature and high-humidity conditions. To relieve heat stress, however, people rely on fixed facilities such as air conditioners, which can lower the ambient temperature but with the compensation of high cost and energy consumption. Regulating body temperature by passive IR radiation thus has great significance in saving energy and improving the comfort of wearable devices and smart face masks.[50−52] Here, we use the SEBS substrate with multiscale porous structures to realize passive heat dissipation and reduce local temperature of face masks. Figure 2d shows the SEM image of the SEBS substrate intrinsically formed by porous structures with pores mainly in the scale of 0.2−7 μm. Such micron-scale porous structures can effectively scatter the visible light (with wavelength of 400−800 nm) and allow mid-IR human body radiation (mainly ranging from 7 to 14 μm) to pass through,[51] giving rise to a passive-cooling property of our RF transponder. As shown in Figure 2e, the wireless harmonic transponder can effectively reduce the local temperature of the smart face mask by about 3 °C when wearing it in an outside environment for 30 min. Without additional cost and energy consumption, the passive-cooling capability mitigates the potential threat of heat stress and widens the practical implementation of the proposed smart face mask in scorching weather. Another principal performance target of face mask materials is high air permeability or breathability. The human body needs to exchange about 500 mL of air in each breath.[53] Therefore, qualified face mask materials are supposed to offer satisfactory air permeability to reduce adverse reactions caused by poor breathing, such as hypoxia and asphyxia. Our soft RF transponder taking advantage of high air permeability of the porous SEBS substrate will not cause any respiratory burden. As shown in Figure 2f, the differential pressure drop across the SEBS substrate is 50.97 Pa/cm^2, which is comparable to that of a commercial face mask (48.44 Pa/cm^2, measured from HDX N95 respirator mask); those pressure drops are tested under a high airflow rate of 8 L/min and through a 25 mm diameter sample test holder. Current smart face masks, on the contrary, typically use nonporous PCBs and PDMS,[5,7−9,21,27] whose

https://doi.org/10.1021/acsnano.1c11041
ACS Nano 2022, 16, 5874−5884

pressure drops far exceed the range of the instrument (100 Pa/cm^2). This comparison shows the distinction of the proposed smart face mask equipped with a SEBS-AgNWs/PEDOT:PSS-based harmonic transponder, namely, providing eminent breathability and wearing comfort. Meanwhile, the multiscale porous structures of SEBS could block most bacteria (with diameters of 0.5−5 μm) and dust (at the micron scale) and, moreover, provide sufficient water resistance.[30] The harmonic transponder with a water-resistant property can thus prevent droplets generated by breath and cough from staying on its surface for a long time and facilitate the possibility of cleaning with water, which favors its reusability. Thanks to the prestretching (prestrain = 100%) process, crumpled structures formed on the surface by AgNWs and PEDOT:PSS (Figure 2b) can disperse the strain and stress under large deformation, so that the resistance change of the conductive materials is diminutive, endowing the transponder tag with excellent tensile, bending, and torsional stability. The resistance change is 11.2% under 50% strain, 6.6% under 1 mm radius bending, and 10.9% under 180° torsional deformation, respectively, as shown in Figure 2g−i. Here, the slight resistance change is due to the deformation of the conductive path under a large strain, and the deviation (obtained from 3 different samples) comes from the individual differences. These measurements may cover the deformations of smart face masks in general use, such as pulling, folding, rubbing, and crumpling. As a matter of fact, since the face masks generally made of nonwoven fabrics are barely stretchable, the deformation or strain applied on the transponder tag is relatively small under normal working conditions. This may lead to negligible resistance changes and deviations, and, thus, the sensing performance of the harmonic transponder is not affected. In addition, the resistance of AgNWs/PEDOT:PSS could be restored after the deformation is removed, further enhancing the endurance and reliability of the harmonic transponder.

Design and Demonstration of Fully-Passive Wireless Smart Face Masks. The geometry and equivalent circuit diagram of the soft harmonic sensor conformally attached to the smart face mask are presented in Figure 1c,d, respectively, which comprises a tree-shaped meander-line antenna resonating at the fundamental frequency (1.6 GHz), a frequency multiplier, and a curved inverted-F antenna resonating at the second-harmonic frequency (3.2 GHz). The coplanar waveguide (CPW)-type transmission lines are used to link the antennas and the frequency multiplier, forming a passive harmonic transponder with a compact size (58 mm × 33 mm; design parameters are detailed in Section S3). Figure 3a,d shows the photographs of the fabricated antenna (left), made of PEDOT:PSS-coated AgNWs and SEBS substrate (with thickness of 0.2 mm), and the measurement of reflection coefficients (right) for the tree-shaped monopole antenna and the curved inverted-F antenna. We note that the PEDOT:PSS-coated AgNWs exhibit excellent conductivity and electrical stability, suitable for the design of RF antennas and circuits in wireless tags. To study the human body's parasitic effects, the flexible and stretchable antennas are first attached to the human body and then lifted with an air gap of d (mm). Figure 3b,e, respectively, plots the reflection coefficients (S_{11}) for the tree-shaped monopole antenna and the curved inverted-F antenna, with the air gap (d) between the antenna and the human body varied from 0 mm (conformal to the skin) to 10 mm. The measured reflection coefficients (solid lines) are in good agreement with the simulated ones (dashed lines).[54] We note that the conductive materials (AgNWs and PEDOT:PSS) and the SEBS substrate may not have a negative impact on the reflection coefficients of the designed monopole and inverted-F antennas, as they achieve excellent S_{11} of less than −25 dB at their resonant frequencies. It is seen from Figure 3b,e that the tree-shaped and curved inverted-F antennas, if placed away from the human body ($d \geq 10$ mm), can resonate at 1.6 GHz (with a −10 dB bandwidth of 280 MHz) and 3.2 GHz (with a −10 dB bandwidth of 680 MHz), respectively. The harmonic transponder receives the interrogation signal at a certain fundamental frequency (1.6 GHz here) sent from the reader through the monopole antenna, generating the second harmonic (3.2 GHz) through the Schottky diode-based passive frequency multiplier and transmitting the frequency-modulated signal (3.2 GHz) to the reader or sniffer through the inverted-F antenna (Figure 1a,d). The information on coughs and mask-wearing conditions is encoded in the emitted second harmonic, that is, received signal strength indicator (RSSI) at 3.2 GHz. In general, when a cough occurs or face masks are not worn (including incorrect wearing of a face mask), the distance between the face mask and human body is close to or >10 mm such that the reader's receiving antenna or sniffer can detect pulsed second harmonic when coughing or continuous second-harmonic signal if the mask is worn improperly. The above scenarios are regarded as the "active" state of the harmonic tag. On the other hand, when the antennas get closer to the human head ($d \leq 5$ mm), indicating the noncough and proper mask-wearing condition, noticeable shifts in antennas' resonant frequencies are observed, that is, the resonance frequency of the tree-shaped monopole is downshifted from 1.6 to 0.96 GHz and that of the inverted-F antenna is downshifted from 3.2 to 1.8 GHz. These lead to disappearance of harmonic signals, and thus detectable signals are below the noise floor of the receiver. This scenario is therefore specified as the "rest" state of the harmonic tag. Figure 3c,f reports the E-plane and H-plane radiation patterns of the tree-shaped monopole antenna at 1.6 GHz and the inverted-F antenna at 3.2 GHz, respectively. The measurement results match quite well to the simulated ones.[54] The tree-shaped monopole has the maximum gain of −2.16 dBi in the broadside direction and the half-power beamwidth (HPBW) of 95°. The curved inverted-F antenna has the maximum gain of −0.52 dBi in the broadside direction and the HPBW of 85° on the E-plane. At resonances, the radiation efficiency of tree-shaped monopole is ∼39% and that of the inverted-F antenna is ∼53%; these values obtained from the SEBS-AgNWs/PEDOT:PSS-based antennas are slightly lower than those of their counterparts made of metals and PCB substrates, primarily due to the relatively high sheet resistance of AgNWs hybrid (∼1 Ω/□) compared with that of commonly used metals such as copper.

The frequency multiplier, converting the fundamental tone at 1.6 GHz to its second harmonic at 3.2 GHz, is based on the lumped-element-based matching networks and filters connected to a Schottky diode (SMS7621, Skyworks Solutions Inc.). The circuit diagram and photograph of the frequency multiplier are shown in Figures 1d and 3g, respectively, with details described in Section S3. The lumped elements (L and C) are connected to the AgNWs/PEDOT:PSS conductive materials through the conductive epoxy (CW2400, Chemtronics). The input and output of the frequency multiplier are connected to the CPW-type transmission lines, which have a characteristic impedance of 50 Ω, matched to the input impedance of the tree-shaped antenna and the inverted-F

https://doi.org/10.1021/acsnano.1c11041
ACS Nano 2022, 16, 5874−5884

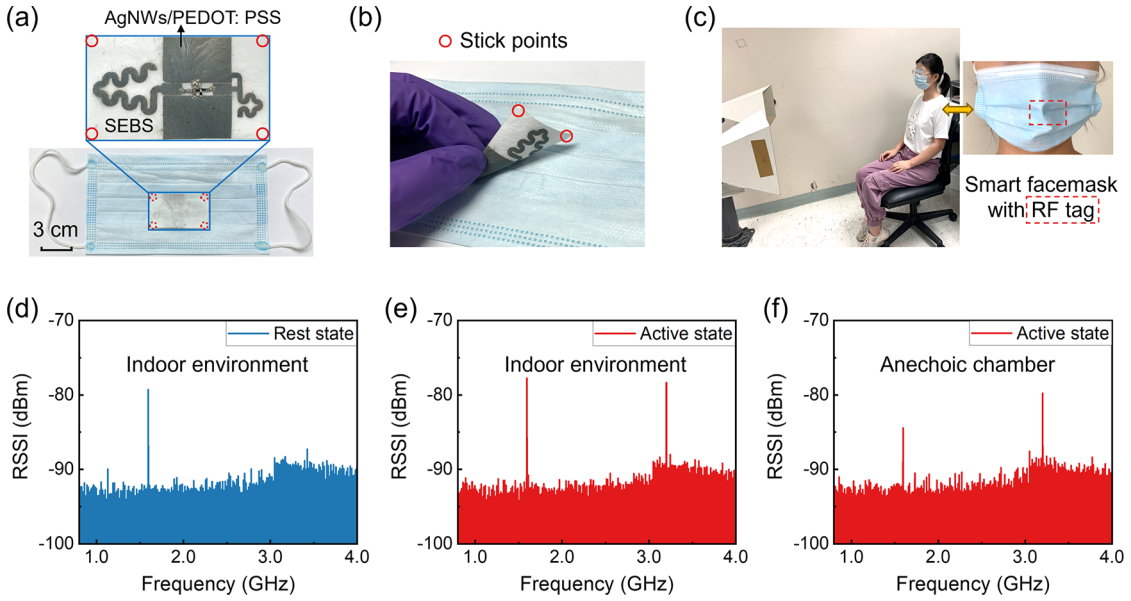

Figure 4. (a) Photograph of the assembled smart face mask where the harmonic sensor is pasted on the inner layer of a surgical face mask. (b) Photograph of RF transponder tag partially torn from the face mask, which is eligible for repeated use. (c) Experimental setup of continuous cough and mask-wearing monitoring in a noisy indoor environment, where the experimenter wears the smart face mask continuously interrogated by the continuous-wave signal from the transmitting antenna. (d) Measured RSSI of the rest-state smart mask in an indoor environment, from which no second-harmonic signal can be observed. (e) and (f) The measured RSSI of the active-state smart mask when it operates in an indoor and a reflectionless environment (i.e., anechoic chamber), respectively. The second-harmonic signals which indicate cough and/or mask not properly worn are observed.

antenna (Figure S4). For testing purposes, the input and output terminals of the frequency multiplier are, respectively, connected to the analog signal generator (N5173B, Keysight) and the spectrum analyzer (E4440A, Agilent). Figure 3h reports the output spectrum of the frequency multiplier at 0 dBm input power, showing a satisfactory conversion loss of 25.8 dB; here, the conversion loss is defined as the power at the input fundamental frequency in dBm subtracted by power at the output second-harmonic frequency in dBm. Figure 3i plots the conversion loss of the frequency multiplier at different input power levels and an input frequency of 1.6 GHz (blue line) and that of the same device at different input frequencies and an input power of 0 dBm (red line). It is evident from Figure 3i that the conversion loss of the designed frequency multiplier achieves its minimum (~25.8 dB) at around 3.2 GHz, indicating that the CPW-type transmission line formed by conductive AgNWs/PEDOT:PSS and SEBS substrate can support proper functioning of the frequency multiplier.

Figure 4a shows the assembled wireless smart face mask where the SEBS-AgNWs/PEDOT:PSS-based flexible RF harmonic transponder is pasted on a surgical face mask (purchased from Naton Medical Group). Figure 4b is similar to Figure 4a, but illustrating that the RF tag can be easily torn off. We note that this wireless device is reusable by simply tearing it off and reattaching it to a new face mask through the silicone elastomer (Silbione RT GEL 4717 A&B, Elkem), which has been proven effective in ref 55. Figure 4c plots the experimental setup of wireless cough and mask-wearing monitoring in a noisy indoor environment, where the transmitting antenna is connected to the RF signal generator and the receiving antenna is connected to the spectrum analyzer. The experimenter wearing the designed smart face mask sits in the far field of the antennas. As discussed above, only when the smart mask is in the "active" state (i.e., not wearing the mask or coughing), the tree-shaped monopole and inverted-F antennas can resonate at 1.6 and 3.2 GHz, respectively. This enables the harmonic transponder to efficiently receive the interrogation signal at the fundamental frequency and retransmit the second harmonic. The second-harmonic RSSI detected by the reader's receiving antenna would indicate coughing and mask-wearing behaviors. In this experiment, the distance between the transmitting antenna and the harmonic transponder (R_1) is fixed to 0.5 m, the input power at the transmitting antenna is 25 dBm, the transmitting antenna (standard gain horn antenna FR6509, Flam and Russell, Inc.) has a realized gain of 14 dBi at 1.6 GHz, and the receiving antenna (standard gain horn antenna FR6510, Flam and Russell, Inc.) has a realized gain of 18.4 dBi at 3.2 GHz. Figure 4d presents the measured RSSI spectrum for the "rest" state of the smart face mask in the indoor environment, where the distance between the receiving antenna and the soft RF tag (R_2) is 0.5 m. As can be seen from Figure 4d, there is no indication for the second-harmonic signal, suggesting that the mask is properly worn and cough does not occur. Figure 4e,f presents the measured RSSI spectrum for the "active" state of smart face mask in the same background and a reflectionless environment (i.e., anechoic chamber), respectively; here, R_2 = 0.5 m. We note that a typical indoor environment inevitably has unwanted clutters, crosstalks, and self-jamming; all these effects interfere the fundamental-frequency RSSI and affect the resolvability and detectability. These electromagnetic interferences, however, can be ruled out or significantly suppressed at harmonic frequencies due to the frequency orthogonality between the transmitted and received RF signals, and therefore the second-harmonic RSSI can be exploited to robustly and accurately detect coughing and mask-wearing conditions (Figure 4e,f).

https://doi.org/10.1021/acsnano.1c11041
ACS Nano 2022, 16, 5874−5884

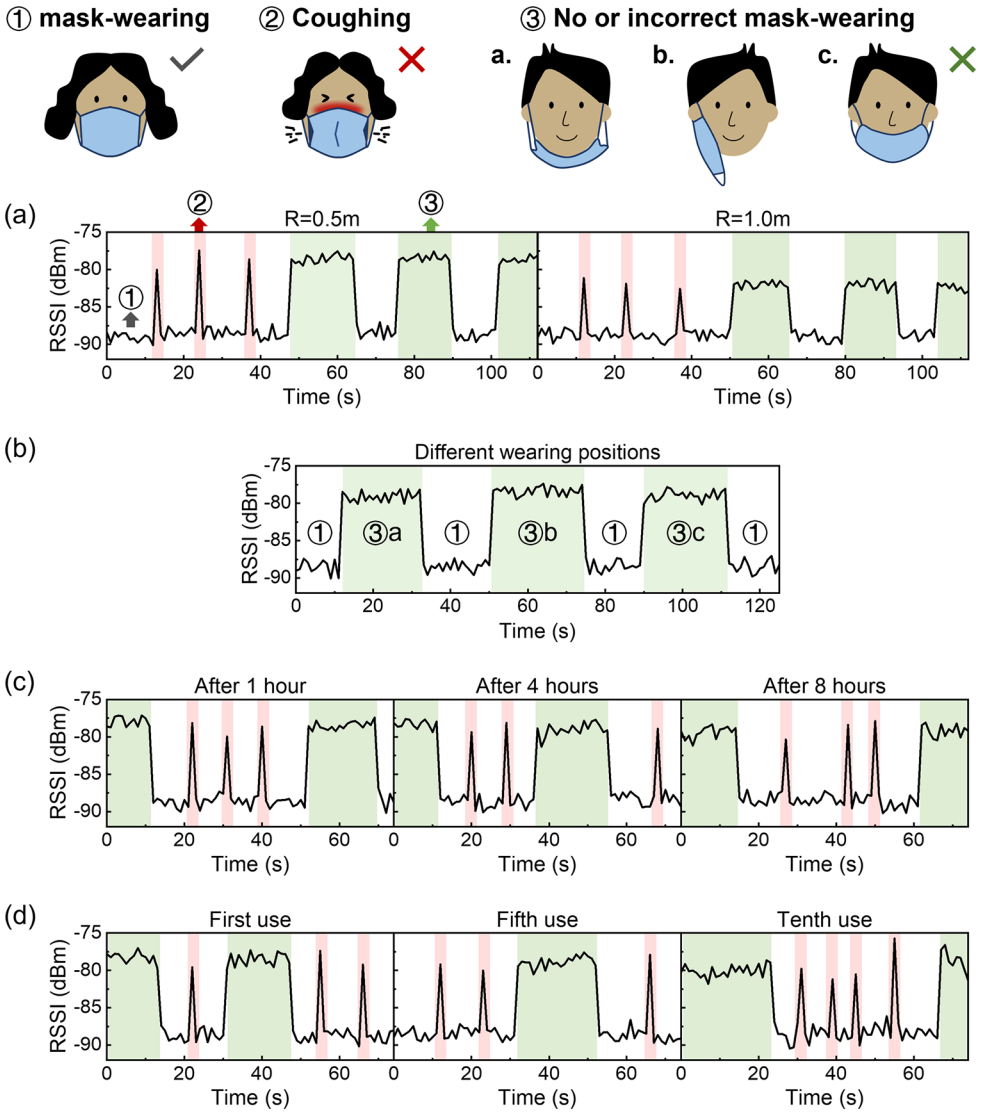

Figure 5. Time-series RSSI signals of the SEBS-AgNWs/PEDOT:PSS-based smart face mask (a) with different tag-to-receiving antenna distances R_2, (b) with different wearing positions, (c) after 1, 4, and 8 h of use, and (d) at first, fifth and tenth use. The harmonic peaks (red bars) and rectangular functions (green bars) in time series of RSSI, respectively, indicate coughing and the mask not worn properly. We see from (c) and (d) that the proposed smart face mask exhibits excellent reliability and durability.

Figure 5a plots the time-series RSSI from the smart mask at different tag-to-receiving antenna distances (R_2). It is seen from Figure 5a that although the harmonic RSSI decreases with increasing R_2 due to the increased radio wave propagation loss, similar patterns are obtained in spite of changes in the interrogation distance. From the measured harmonic RSSI, a distinct second-harmonic peak appears when coughing occurs. The successive appearance of second-harmonic signals (i.e., a rectangular function in time series of RSSI) indicates that the face mask is not properly worn (i.e., there is an air gap between the harmonic tag and face). On the other hand, the absence of second-harmonic RSSI denotes that the mask is properly worn, with an air gap <5 mm. Here, we also investigate the response of the smart face mask to different improper mask-wearing scenarios, including: (a) a mask is tucked under the chin, and the nose and mouth are not covered; (b) hanging a mask off one ear; (c) wearing a mask under the nose, as shown in Figure 5b. From the measurement results, we find that the harmonic transponder would emit a continuous second-harmonic signal as an alarm in all the different improper wearing behaviors. Breathability against dry/wet contacts, high temperature, and RH inside the mask is critically relevant to facilitate mask-wearing. Figure 5c presents continuous monitoring results for coughing and mask-wearing status after 1, 4, and 8 h of usage. It is evident that long-duration wearing does not affect the accuracy and sensitivity of the wireless smart face mask. The results verify the robustness and durability resulting from the PEDOT:PSS passivation layer, which isolates the AgNWs from the air and therefore improves the electrical stability. Meanwhile, the smart face mask offers superior wearing comfort for long-term wearing, owing to its excellent flexibility, high breathability, and passive-cooling capability in light of the ultrasoft and multiscale porous nature of the SEBS substrate. Here, the reusability of the SEBS-AgNWs/PEDOT:PSS-based harmonic tag is demonstrated by repeating the use of RF tags on face masks for 10 times. Figure 5d shows the measured time-series second-harmonic RSSI of the harmonic transponder for its first, fifth, and 10th uses. We see from Figure 5d that the performance of the transponder sensor is not influenced by the times of use. This reveals that the harmonic

https://doi.org/10.1021/acsnano.1c11041
ACS Nano 2022, 16, 5874−5884

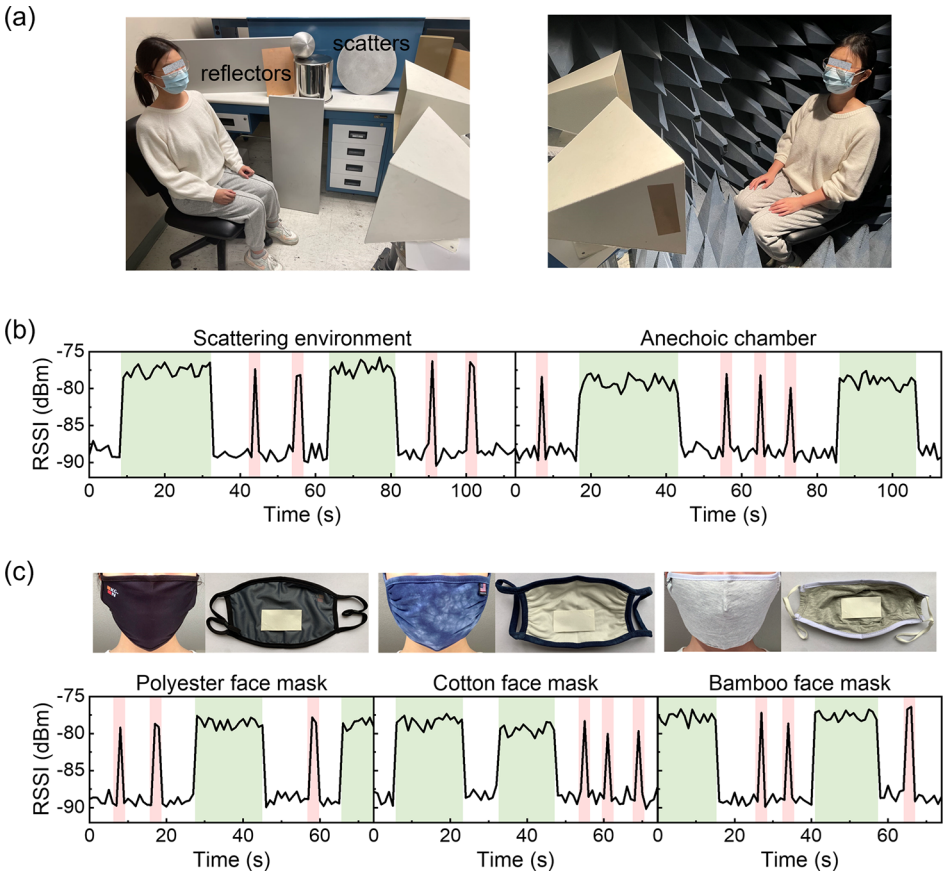

Figure 6. (a) Experimental setup of continuous cough and mask-wearing monitoring in a rich-scattering environment where there are multiple large-RCS scatters (left) and a no-reflection anechoic chamber (right). (b) Measured harmonic RSSI signals in the rich-scattering environment and the anechoic chamber. (c) Time-series harmonic RSSI signals measured from the same RF transponder attached onto different types of face masks.

sensor tag can be reusable for at least 10 times (see Section S4 for more details). Such highly reliable and durable sensing performance is enabled by the excellent electrical stability of PEDOT:PSS-coated AgNWs, noise-immune harmonic sensing technique, and the "binary" sensing scheme where the "active" state and the "rest" state can be easily differentiated from each other. The reusability and durability of the soft harmonic tag is also promoted by its water-resistant capability, which makes the RF tag insusceptible to a humidity environment and droplets induced by coughing (refer to ref 30 and Section S5).

To evaluate the immunity of the smart face mask to electromagnetic interferences, we also measure the harmonic RSSI in rich-scattering environments where multiple metallic scatters with large radar cross sections (RCS) are present (Figure 6a). Figure 6b compares the time-series harmonic RSSI pattern measured in a rich-scattering environment (left panel) and that measured in an anechoic chamber (right panel). We find that the time-series patterns of the two measurement conditions are very similar, for which cough frequency and mask-wearing status can be clearly identified without being affected by clutters and multipath scattering events. This is because the detected second-harmonic signal is exclusively generated by the harmonic transponder and is not interfered by the interrogation signal and background noises. The measurement results in Figures 5a–d and 6b are based on the surgical face mask (from Naton Medical Group) made of nonwoven fabric layers. In the following, we will integrate the soft harmonic transponder with different types of face masks, including the polyester face mask (from K&N Engineering, Inc.), the cotton face mask (from Tart Collections), and the bamboo face mask (from NxTSTOP Apparel). The Silbione allows effective bonding between the SEBS substrate and various materials used in face masks (e.g., nonwoven, cotton, and polyester fabrics). The second-harmonic RSSI patterns measured with these different face mask types show that the RF transponder sensor performs well on a variety of masks from different manufacturers (Figure 6c).

Finally, we should note that the RF harmonic transponder could also include the energy-efficient radio frequency identification (RFID) chip with memory and the backscatter transistor such that identification can be performed along with sensing.[56−60] The ID data path is picked up by the RFID reader, so the proposed smart face mask can be either used as a pure sensor (chipless) or sensor with ID (chip-enabled) underneath the standard RFID operating protocols. In addition, the recorded cough events, including the amplitude and number of peaks in the time-domain data (Figures 5 and 6), can be analyzed using intelligent algorithms, such as machine learning and deep learning methods,[44−46] for recognizing features (e.g., dry cough, productive wet cough, or chesty cough) that correspond to different respiratory diseases. Compared to current acoustic approaches that detect cough sounds using digital voice recorders,[61−63] the RF sensing technique has several advantages. First, acoustic cough monitoring approaches suffer from confusion with background noises and parasitic patient sounds that are not related to the

https://doi.org/10.1021/acsnano.1c11041
ACS Nano 2022, 16, 5874−5884

disease transmission (e.g., throat clearing, humming, or laughing). Second, cough detection using sound could lose important details, such as whether the person is wearing a face mask when coughing. Unlike optical approaches, such as optical camera and face recognition techniques,[64−66] the proposed RF approach does not have any privacy concerns, while providing comparable or even improved accuracy and reliability. In addition to monitoring coughs and identifying mask-wearing status to prevent the spread of infectious respiratory diseases, the wireless soft harmonic transponder may find many applications in smart wearables and IoT devices. For instance, the transponder can act as a motion or gesture sensor which detects the movement of knees, elbows, fingers, and so on, since any movement or bending that alters the resonant frequency of the soft antennas can lead to modulation of harmonic strengths.

CONCLUSION

To sum up, we have designed, fabricated, and characterized the wireless smart face mask embedded with a soft and battery-free RF harmonic transponder that enables continuous, real-time wireless monitoring of coughs and mask wearing. Unlike the current smart face masks, the antennas and circuit of the RF transponder are manufactured based on the spray-printed AgNWs/PEDOT:PSS and multiscale porous SEBS substrate, which can be ultrasoft, flexible, stretchable, and, most importantly, passive-cooling and breathable for providing long-term wearing comfort. Also, the AgNWs coated with the PEDOT:PSS passivation layer exhibit highly stable electrical properties in a moisture environment, ensuring reliability and practicability of the proposed smart face mask. Moreover, the soft RF transponder attached to the face mask through silicone elastomers is easy to use and reusable, leading to an environmentally friendly solution. Our wireless measurement results performed in the realistic indoor environment show that coughing and improper mask-wearing can be clearly indicated from the recorded second-harmonic RSSI pattern. We envision that the proposed wireless smart face mask may not only mitigate the spread of infectious respiratory diseases during a pandemic but also facilitate health condition monitoring in clinical practice, telemedicine, and healthcare IoT.

METHODS

Fabrication of Harmonic Sensor. SEBS pellets (H1062; Asahi Kasei) were first dissolved in chloroform (60 mg·mL^{-1}). Then, the solution was mixed with 40 vol % isopropyl alcohol (IPA) and sonicated to clear. The clear solution was casted on aluminum foil and dried in the fume hood overnight to form a porous SEBS substrate. AgNW (Ag NW-L50; ACS Material) solution was diluted by IPA by 1:10 wt % and then spray-printed onto a prestretched SEBS substrate (prestrain = 100%) by an air-brush with the assist of a shadow mask. The mask is made of water-soluble tape and patterned by a CO_2 laser (ULS 2.30 system). The PEDOT:PSS solution (Sigma-Aldrich) was diluted by IPA 1:1 wt % and spray-printed using the same steps as AgNWs. The sprayed concentrations of as-prepared AgNWs and PEDOT:PSS were 1 and 0.5 mL per 25 cm^2, respectively. The conductive material was sprayed on the SEBS substrate at temperature 60 °C on a hot plate, and then the sensor was baked in the oven under 60 °C overnight. The mask was removed from the sensor and released to finish sensor fabrication.

Characterizations and Measurements. The SEM images (Figure 2b,d) were taken by an FEI Quanta 600 system. The thermal image (Figure 2e) was taken by an IR camera (FLIR E6). The differential pressure drops (Figure 2f) were tested by a Medical Mask Differential Pressure Tester, SATATON T438, Sataton Instruments Technology Co., Ltd. Shanghai, China. The resistance changes of the transponder under deformation (Figure 2g−i) were determined by a digital source meter (2604B; Keithley Instruments).

ASSOCIATED CONTENT

Supporting Information

The Supporting Information is available free of charge at https://pubs.acs.org/doi/10.1021/acsnano.1c11041.

Sections S1: Biosafety of PEDOT:PSS-coated AgNWs. S2: Estimation of the thickness of conductive materials. S3: Design of the wireless harmonic transponder. S4: Reusability of the harmonic transponder sensor. S5: Water-resistant ability of the transponder tag (PDF)

AUTHOR INFORMATION

Corresponding Authors

Zheng Yan − *Department of Mechanical and Aerospace Engineering and Department of Biomedical, Biological, and Chemical Engineering, University of Missouri, Columbia, Missouri 65211, United States;* orcid.org/0000-0001-5968-0934; Email: yanzheng@missouri.edu

Pai-Yen Chen − *Department of Electrical and Computer Engineering, University of Illinois at Chicago, Chicago, Illinois 60607, United States*; Email: pychen@uic.edu

Authors

Zhilu Ye − *Department of Electrical and Computer Engineering, University of Illinois at Chicago, Chicago, Illinois 60607, United States;* orcid.org/0000-0002-0017-6722

Yun Ling − *Department of Mechanical and Aerospace Engineering, University of Missouri, Columbia, Missouri 65211, United States*

Minye Yang − *Department of Electrical and Computer Engineering, University of Illinois at Chicago, Chicago, Illinois 60607, United States*

Yadong Xu − *Department of Biomedical, Biological, and Chemical Engineering, University of Missouri, Columbia, Missouri 65211, United States*

Liang Zhu − *Department of Electrical and Computer Engineering, University of Illinois at Chicago, Chicago, Illinois 60607, United States*

Complete contact information is available at: https://pubs.acs.org/10.1021/acsnano.1c11041

Author Contributions

‖These authors contributed equally to this work.

Notes

The authors declare no competing financial interest.

ACKNOWLEDGMENTS

This material is based upon work supported by the National Science Foundation under grant no. ECCS-1914420 (P.-Y.C.) and grant no. CMMI-2045101 (Z.Y.).

REFERENCES

(1) WHO *Coronavirus (COVID-19) Dashboard.* https://covid19.who.int (accessed 2022-03-09).

(2) Jefferson, T.; Mar, C. B. D.; Dooley, L.; Ferroni, E.; Al-Ansary, L. A.; Bawazeer, G. A.; van Driel, M. L.; Jones, M. A.; Thorning, S.; Beller, E. M.; Clark, J.; Hoffmann, T. C.; Glasziou, P. P.; Conly, J. M. Physical Interventions to Interrupt or Reduce the Spread of

Respiratory Viruses. *Cochrane Database Syst. Rev.* **2020**, No. 11, CD006207.
(3) Leung, N. H. L.; Chu, D. K. W.; Shiu, E. Y. C.; Chan, K.-H.; McDevitt, J. J.; Hau, B. J. P.; Yen, H.-L.; Li, Y.; Ip, D. K. M.; Peiris, J. S. M.; Seto, W.-H.; Leung, G. M.; Milton, D. K.; Cowling, B. J. Respiratory Virus Shedding in Exhaled Breath and Efficacy of Face Masks. *Nat. Med.* **2020**, *26* (5), 676−680.
(4) Worby, C. J.; Chang, H.-H. Face Mask Use in the General Population and Optimal Resource Allocation during the COVID-19 Pandemic. *Nat. Commun.* **2020**, *11* (1), 4049.
(5) Pan, L.; Wang, C.; Jin, H.; Li, J.; Yang, L.; Zheng, Y.; Wen, Y.; Tan, B. H.; Loh, X. J.; Chen, X. Lab-on-Mask for Remote Respiratory Monitoring. *ACS Materials Lett.* **2020**, *2* (9), 1178−1181.
(6) Liu, Z.; Tian, B.; Zhang, B.; Liu, J.; Zhang, Z.; Wang, S.; Luo, Y.; Zhao, L.; Shi, P.; Lin, Q.; Jiang, Z. A Thin-Film Temperature Sensor Based on a Flexible Electrode and Substrate. *Microsyst Nanoeng* **2021**, *7* (1), 1−14.
(7) Fois, A.; Tocco, F.; Dell'Osa, A.; Melis, L.; Bertelli, U.; Concu, A.; Manuello Bertetto, A.; Serra, C. Innovative Smart Face Mask to Protect Workers from COVID-19 Infection. Proceedings from the *2021 IEEE International Symposium on Medical Measurements and Applications (MeMeA)*, June 23−25, 2021, Neuchâtel, Switzerland; IEEE: New York, 2021; pp 1−6.
(8) Kalavakonda, R. R.; Masna, N. V. R.; Bhuniaroy, A.; Mandal, S.; Bhunia, S. A Smart Mask for Active Defense Against Coronaviruses and Other Airborne Pathogens. *IEEE Consumer Electronics Magazine* **2021**, *10* (2), 72−79.
(9) Xia, K.; Li, X.; Li, X.; Liu, Y.; Zhang, H.; Hou, R. Intelligent Anti-epidemic Mask Based on KF and ECF Fusion Algorithm. *Electron. Lett.* , **2021**, DOI: 10.1049/ell2.12240.
(10) Thiyagarajan, K.; Rajini, G. K.; Maji, D. Flexible, Highly Sensitive Paper-Based Screen Printed MWCNT/PDMS Composite Breath Sensor for Human Respiration Monitoring. *IEEE Sensors Journal* **2021**, *21* (13), 13985−13995.
(11) Ghatak, B.; Banerjee, S.; Ali, S. B.; Bandyopadhyay, R.; Das, N.; Mandal, D.; Tudu, B. Design of a Self-Powered Smart Mask for COVID-19. *arXiv (Medical Physics)*, May 17, 2020, 2005.08305, ver. 1. https://arxiv.org/abs/2005.08305 (accessed on August 10th, 2021).
(12) Li, J.; Long, Y.; Yang, F.; Wang, X. Respiration-Driven Triboelectric Nanogenerators for Biomedical Applications. *EcoMat* **2020**, *2* (3), e12045.
(13) Cheng, Y.; Wang, C.; Zhong, J.; Lin, S.; Xiao, Y.; Zhong, Q.; Jiang, H.; Wu, N.; Li, W.; Chen, S.; Wang, B.; Zhang, Y.; Zhou, J. Electrospun Polyetherimide Electret Nonwoven for Bi-Functional Smart Face Mask. *Nano Energy* **2017**, *34*, 562−569.
(14) Sharma, P.; Hui, X.; Zhou, J.; Conroy, T. B.; Kan, E. C. Wearable Radio-Frequency Sensing of Respiratory Rate, Respiratory Volume, and Heart Rate. *npj Digit. Med.* **2020**, *3* (1), 1−10.
(15) Hui, X.; Kan, E. C. Monitoring Vital Signs over Multiplexed Radio by Near-Field Coherent Sensing. *Nat. Electron* **2018**, *1* (1), 74−78.
(16) Shi, M.; Wu, H.; Zhang, J.; Han, M.; Meng, B.; Zhang, H. Self-Powered Wireless Smart Patch for Healthcare Monitoring. *Nano Energy* **2017**, *32*, 479−487.
(17) Jalal, A.; Batool, M.; Kim, K. Sustainable Wearable System: Human Behavior Modeling for Life-Logging Activities Using K-Ary Tree Hashing Classifier. *Sustainability* **2020**, *12* (24), 10324.
(18) Zhao, Y.; Wang, B.; Hojaiji, H.; Wang, Z.; Lin, S.; Yeung, C.; Lin, H.; Nguyen, P.; Chiu, K.; Salahi, K.; Cheng, X.; Tan, J.; Cerrillos, B. A.; Emaminejad, S. A Wearable Freestanding Electrochemical Sensing System. *Science Advances* **2020**, *6* (12), eaaz0007.
(19) Wang, T.; Zhang, Y.; Liu, Q.; Cheng, W.; Wang, X.; Pan, L.; Xu, B.; Xu, H. A Self-Healable, Highly Stretchable, and Solution Processable Conductive Polymer Composite for Ultrasensitive Strain and Pressure Sensing. *Adv. Funct. Mater.* **2018**, *28* (7), 1705551.
(20) Wang, Z.; Wang, T.; Zhuang, M.; Xu, H. Stretchable Polymer Composite with a 3D Segregated Structure of PEDOT:PSS for Multifunctional Touchless Sensing. *ACS Appl. Mater. Interfaces* **2019**, *11* (48), 45301−45309.
(21) Yang, G.; Jiang, M.; Ouyang, W.; Ji, G.; Xie, H.; Rahmani, A. M.; Liljeberg, P.; Tenhunen, H. IoT-Based Remote Pain Monitoring System: From Device to Cloud Platform. *IEEE Journal of Biomedical and Health Informatics* **2018**, *22* (6), 1711−1719.
(22) Keum, D. H.; Kim, S.-K.; Koo, J.; Lee, G.-H.; Jeon, C.; Mok, J. W.; Mun, B. H.; Lee, K. J.; Kamrani, E.; Joo, C.-K.; Shin, S.; Sim, J.-Y.; Myung, D.; Yun, S. H.; Bao, Z.; Hahn, S. K. Wireless Smart Contact Lens for Diabetic Diagnosis and Therapy. *Science Advances* **2020**, *6* (17), eaba3252.
(23) Wang, H.; Han, M.; Song, Y.; Zhang, H. Design, Manufacturing and Applications of Wearable Triboelectric Nanogenerators. *Nano Energy* **2021**, *81*, 105627.
(24) Wen, D.-L.; Sun, D.-H.; Huang, P.; Huang, W.; Su, M.; Wang, Y.; Han, M.-D.; Kim, B.; Brugger, J.; Zhang, H.-X.; Zhang, X.-S. Recent Progress in Silk Fibroin-Based Flexible Electronics. *Microsyst Nanoeng* **2021**, *7* (1), 1−25.
(25) Stanford, M. G.; Yang, K.; Chyan, Y.; Kittrell, C.; Tour, J. M. Laser-Induced Graphene for Flexible and Embeddable Gas Sensors. *ACS Nano* **2019**, *13* (3), 3474−3482.
(26) Gao, Y.; Zhang, Y.; Wang, X.; Sim, K.; Liu, J.; Chen, J.; Feng, X.; Xu, H.; Yu, C. Moisture-Triggered Physically Transient Electronics. *Science Advances* **2017**, *3* (9), e1701222.
(27) Gao, Z.; Lou, Z.; Chen, S.; Li, L.; Jiang, K.; Fu, Z.; Han, W.; Shen, G. Fiber Gas Sensor-Integrated Smart Face Mask for Room-Temperature Distinguishing of Target Gases. *Nano Res.* **2018**, *11* (1), 511−519.
(28) Chow, E. J.; Schwartz, N. G.; Tobolowsky, F. A.; Zacks, R. L. T.; Huntington-Frazier, M.; Reddy, S. C.; Rao, A. K. Symptom Screening at Illness Onset of Health Care Personnel With SARS-CoV-2 Infection in King County, Washington. *JAMA* **2020**, *323* (20), 2087−2089.
(29) Korpáš, J.; Sadloňová, J.; Vrabec, M. Analysis of the Cough Sound: An Overview. *Pulmonary Pharmacology* **1996**, *9* (5), 261−268.
(30) Xu, Y.; Sun, B.; Ling, Y.; Fei, Q.; Chen, Z.; Li, X.; Guo, P.; Jeon, N.; Goswami, S.; Liao, Y.; Ding, S.; Yu, Q.; Lin, J.; Huang, G.; Yan, Z. Multiscale Porous Elastomer Substrates for Multifunctional On-Skin Electronics with Passive-Cooling Capabilities. *Proc. Natl. Acad. Sci. U.S.A.* **2020**, *117* (1), 205−213.
(31) Balint, R.; Cassidy, N. J.; Cartmell, S. H. Conductive Polymers: Towards a Smart Biomaterial for Tissue Engineering. *Acta Biomaterialia* **2014**, *10* (6), 2341−2353.
(32) Lehmann, S. G.; Gilbert, B.; Maffeis, T. G.; Grichine, A.; Pignot-Paintrand, I.; Clavaguera, S.; Rachidi, W.; Seve, M.; Charlet, L. In Vitro Dermal Safety Assessment of Silver Nanowires after Acute Exposure: Tissue vs. Cell Models. *Nanomaterials* **2018**, *8* (4), 232.
(33) Zhu, L.; Alkhaldi, N.; Kadry, H. M.; Liao, S.; Chen, P.-Y. A Compact Hybrid-Fed Microstrip Antenna for Harmonics-Based Radar and Sensor Systems. *IEEE Antennas and Wireless Propagation Letters* **2018**, *17* (12), 2444−2448.
(34) Huang, H.; Tao, L.; Liu, F.; Ji, L.; Hu, Y.; Cheng, M. M.-C.; Chen, P.-Y.; Akinwande, D. Chemical-Sensitive Graphene Modulator with a Memory Effect for Internet-of-Things Applications. *Microsyst Nanoeng* **2016**, *2* (1), 1−9.
(35) Zhu, L.; Farhat, M.; Chen, Y.-C.; Salama, K. N.; Chen, P.-Y. A Compact, Passive Frequency-Hopping Harmonic Sensor Based on a Microfluidic Reconfigurable Dual-Band Antenna. *IEEE Sensors Journal* **2020**, *20* (21), 12495−12503.
(36) Zhu, L.; Huang, H.; Cheng, M. M.-C.; Chen, P.-Y. Compact, Flexible Harmonic Transponder Sensor With Multiplexed Sensing Capabilities for Rapid, Contactless Microfluidic Diagnosis. *IEEE Transactions on Microwave Theory and Techniques* **2020**, *68* (11), 4846−4854.
(37) Huang, H.; Chen, P.-Y.; Hung, C.-H.; Gharpurey, R.; Akinwande, D. A Zero Power Harmonic Transponder Sensor for Ubiquitous Wireless ML Liquid-Volume Monitoring. *Sci. Rep* **2016**, *6* (1), 18795.

https://doi.org/10.1021/acsnano.1c11041
ACS Nano 2022, 16, 5874−5884

(38) Huang, H.; Sakhdari, M.; Hajizadegan, M.; Shahini, A.; Akinwande, D.; Chen, P.-Y. Toward Transparent and Self-Activated Graphene Harmonic Transponder Sensors. *Appl. Phys. Lett.* **2016**, *108* (17), 173503.
(39) Rasilainen, K.; Ilvonen, J.; Hannula, J.-M.; Viikari, V. Designing Harmonic Transponders Using Lumped-Component Matching Circuits. *IEEE Antennas and Wireless Propagation Letters* **2017**, *16*, 246−249.
(40) Rasilainen, K.; Ilvonen, J.; Lehtovuori, A.; Hannula, J.-M.; Viikari, V. On Design and Evaluation of Harmonic Transponders. *IEEE Transactions on Antennas and Propagation* **2015**, *63* (1), 15−23.
(41) Hui, X.; Conroy, T. B.; Kan, E. C. Near-Field Coherent Sensing of Vibration With Harmonic Analysis and Balance Signal Injection. *IEEE Transactions on Microwave Theory and Techniques* **2021**, *69* (3), 1906−1916.
(42) Hui, X.; Kan, E. C. No-Touch Measurements of Vital Signs in Small Conscious Animals. *Science Advances* **2019**, *5* (2), eaau0169.
(43) Hui, X.; Kan, E. C. Radio Ranging with Ultrahigh Resolution Using a Harmonic Radio-Frequency Identification System. *Nat. Electron* **2019**, *2* (3), 125−131.
(44) Pahar, M.; Klopper, M.; Warren, R.; Niesler, T. COVID-19 Cough Classification Using Machine Learning and Global Smartphone Recordings. *Computers in Biology and Medicine* **2021**, *135*, 104572.
(45) Van Hirtum, A.; Berckmans, D. Automated Recognition of Spontaneous versus Voluntary Cough. *Medical Engineering & Physics* **2002**, *24* (7−8), 541−545.
(46) Shimon, C.; Shafat, G.; Dangoor, I.; Ben-Shitrit, A. Artificial Intelligence Enabled Preliminary Diagnosis for COVID-19 from Voice Cues and Questionnaires. *J. Acoust. Soc. Am.* **2021**, *149* (2), 1120−1124.
(47) Kim, S. H.; Choi, W. I.; Kim, K. H.; Yang, D. J.; Heo, S.; Yun, D.-J. Nanoscale Chemical and Electrical Stabilities of Graphene-Covered Silver Nanowire Networks for Transparent Conducting Electrodes. *Sci. Rep* **2016**, *6* (1), 33074.
(48) Chung, K. F.; Seiffert, J.; Chen, S.; Theodorou, I. G.; Goode, A. E.; Leo, B. F.; McGilvery, C. M.; Hussain, F.; Wiegman, C.; Rossios, C.; Zhu, J.; Gong, J.; Tariq, F.; Yufit, V.; Monteith, A. J.; Hashimoto, T.; Skepper, J. N.; Ryan, M. P.; Zhang, J.; Tetley, T. D.; Porter, A. E. Inactivation, Clearance, and Functional Effects of Lung-Instilled Short and Long Silver Nanowires in Rats. *ACS Nano* **2017**, *11* (3), 2652−2664.
(49) Courtney, J. M.; Bax, A. Hydrating the Respiratory Tract: An Alternative Explanation Why Masks Lower Severity of COVID-19 Disease. *Biophys. J.* **2021**, *120*, 994.
(50) Zeng, S.; Pian, S.; Su, M.; Wang, Z.; Wu, M.; Liu, X.; Chen, M.; Xiang, Y.; Wu, J.; Zhang, M.; Cen, Q.; Tang, Y.; Zhou, X.; Huang, Z.; Wang, R.; Tunuhe, A.; Sun, X.; Xia, Z.; Tian, M.; Chen, M.; Ma, X.; Yang, L.; Zhou, J.; Zhou, H.; Yang, Q.; Li, X.; Ma, Y.; Tao, G. Hierarchical-Morphology Metafabric for Scalable Passive Daytime Radiative Cooling. *Science* **2021**, *373* (6555), 692−696.
(51) Hsu, P.-C.; Song, A. Y.; Catrysse, P. B.; Liu, C.; Peng, Y.; Xie, J.; Fan, S.; Cui, Y. Radiative Human Body Cooling by Nanoporous Polyethylene Textile. *Science* **2016**, *353* (6303), 1019−1023.
(52) Zhang, X. A.; Yu, S.; Xu, B.; Li, M.; Peng, Z.; Wang, Y.; Deng, S.; Wu, X.; Wu, Z.; Ouyang, M.; Wang, Y. Dynamic Gating of Infrared Radiation in a Textile. *Science* **2019**, *363* (6427), 619−623.
(53) Lord, H.; Yu, Y.; Segal, A.; Pawliszyn, J. Breath Analysis and Monitoring by Membrane Extraction with Sorbent Interface. *Anal. Chem.* **2002**, *74* (21), 5650−5657.
(54) Mohring, B. N.; Gabler, B.; Limbach, M. Antenna In-Situ Performance Analysis for the Hypersonic Flight Vehicle HEXAFLY: Employing Measurement Data in a Simulation Model. *IEEE Antennas and Propagation Magazine* **2021**, *63* (4), 89−99.
(55) Jang, K.-I.; Han, S. Y.; Xu, S.; Mathewson, K. E.; Zhang, Y.; Jeong, J.-W.; Kim, G.-T.; Webb, R. C.; Lee, J. W.; Dawidczyk, T. J.; Kim, R. H.; Song, Y. M.; Yeo, W.-H.; Kim, S.; Cheng, H.; Rhee, S. I.; Chung, J.; Kim, B.; Chung, H. U.; Lee, D.; Yang, Y.; Cho, M.; Gaspar, J. G.; Carbonari, R.; Fabiani, M.; Gratton, G.; Huang, Y.; Rogers, J. A. Rugged and Breathable Forms of Stretchable Electronics with Adherent Composite Substrates for Transcutaneous Monitoring. *Nat. Commun.* **2014**, *5* (1), 4779.
(56) Zaffar, A.; Gul, M.; Mumtaz, R.; Ashraf Khan, A. Development of Decision Support System for Health Care Consultation Using RFID Based NFC Tags for Patient Identification. *IJIEEB* **2016**, *8* (3), 20−30.
(57) Cheng, C.-H.; Kuo, Y.-H. RFID Analytics for Hospital Ward Management. *Flex Serv Manuf J.* **2016**, *28* (4), 593−616.
(58) Sarkka, S.; Viikari, V. V.; Huusko, M.; Jaakkola, K. Phase-Based UHF RFID Tracking With Nonlinear Kalman Filtering and Smoothing. *IEEE Sensors Journal* **2012**, *12* (5), 904−910.
(59) Xu, G.; Sharma, P.; Hysell, D. L.; Kan, E. C. Indoor Object Sensing Using Radio-Frequency Identification with Inverse Methods. *IEEE Sensors Journal* **2021**, 1−1.
(60) Jung, M.; Kim, J.; Noh, J.; Lim, N.; Lim, C.; Lee, G.; Kim, J.; Kang, H.; Jung, K.; Leonard, A. D.; Tour, J. M.; Cho, G. All-Printed and Roll-to-Roll-Printable 13.56-MHz-Operated 1-Bit RF Tag on Plastic Foils. *IEEE Trans. Electron Devices* **2010**, *57* (3), 571−580.
(61) Smith, J. Ambulatory Methods for Recording Cough. *Pulmonary Pharmacology & Therapeutics* **2007**, *20* (4), 313−318.
(62) Spinou, A.; Birring, S. S. An Update on Measurement and Monitoring of Cough: What Are the Important Study Endpoints? *J. Thorac Dis* **2014**, *6*, S728−S734.
(63) Smith, J. Monitoring Chronic Cough: Current and Future Techniques. *Expert Review of Respiratory Medicine* **2010**, *4* (5), 673−683.
(64) Loey, M.; Manogaran, G.; Taha, M. H. N.; Khalifa, N. E. M. A Hybrid Deep Transfer Learning Model with Machine Learning Methods for Face Mask Detection in the Era of the COVID-19 Pandemic. *Measurement* **2021**, *167*, 108288.
(65) Hussain, S.; Yu, Y.; Ayoub, M.; Khan, A.; Rehman, R.; Wahid, J. A.; Hou, W. IoT and Deep Learning Based Approach for Rapid Screening and Face Mask Detection for Infection Spread Control of COVID-19. *Applied Sciences* **2021**, *11* (8), 3495.
(66) Loey, M.; Manogaran, G.; Taha, M. H. N.; Khalifa, N. E. M. Fighting against COVID-19: A Novel Deep Learning Model Based on YOLO-v2 with ResNet-50 for Medical Face Mask Detection. *Sustainable Cities and Society* **2021**, *65*, 102600.

https://doi.org/10.1021/acsnano.1c11041
ACS Nano 2022, 16, 5874−5884